Can. Geotech. J. Downloaded from www.nrcresearchpress.com by UNIVERSITAT POLITECNICA DE CATALUNYA on 04/03/18
For personal use only. This Just-IN manuscript is the accepted manuscript prior to copy editing and page composition. It may differ from the final official version of record.

Use of tire derived aggregate in tunnel cut-and-cover

Luis Medina Rodríguez
Department of Geotechnical Engineering, University of La Coruña
Campus de Elviña, s/n. 15071-La Coruña (Spain). Email: lmedina@udc.es

Marcos Arroyo
Department of Civil and Environmental Engineering, UPC, Barcelona, Spain.
Email: marcos.arroyo@upc.edu

Miguel Martín Cano
Department of I+D+i, SACYR Construcción S.A.
Email: mcano@sacyr.com

Abstract. A case-history is reported in which tire derived aggregate (TDA) was successfully applied to reduce the weight of fill upon a cut-and-cover railway tunnel. Subsequent 3D numerical analyses are used to explore the effect of different assumptions about the constitutive model of the TDA material. Alternative dispositions of TDA around the tunnel section are also examined. Reductions of up to 60% in lining bending moment may be achieved. For the case analyzed the elastic description of the TDA has little influence on tunnel lining loads, although is important for fill settlement estimates.

Keywords: End-of-use tires; TDA; monitoring; numerical modelling; tunnels.

Can. Geotech. J. Downloaded from www.nrcresearchpress.com by UNIVERSITAT POLITECNICA DE CATALUNYA on 04/03/18
For personal use only. This Just-IN manuscript is the accepted manuscript prior to copy editing and page composition. It may differ from the final official version of record.

Introduction

Large quantities of used tires are generated worldwide. For instance, recent figures indicate productions of 12.6 kg/habitant/year for EEUU (RMA 2015), 6.4 kg/habitant/year for EU28 countries (ETRMA 2016) or 8 kg/habitant/year for Japan (JATMA 2016). Because of the environmental risks associated with uncontrolled landfill disposal, policy efforts have been systematically directed to encourage re-use and re-cycling of end-of-life tires. Ideal re-cycling outlets are those in which the inherent properties of waste rubber are put to beneficial use with minimal post-processing cost.

Tire Derived Aggregate (TDA) would appear to fit well into that description, and its use as a recycling outlet is actively promoted, (Cheng 2016). TDA is obtained cutting waste tires into relatively large pieces (25 to 300 mm), a process that is relatively simple and energy-efficient. TDA has desirable properties: it is lightweight, (around 6.5 kN/m^3 after compaction) and has large hydraulic conductivity (Romero et al. 2008), offering as well good thermal insulation and vibration damping potential (Brunet et al. 2016). Civil engineering applications may be derived that employ one or more of those properties (for instance, lightweight, good drainage and damping are all convenient for wall backfills in seismic areas, Xiao et al. 2013). It has been documented (Yoon et al. 2006) that TDA is competitively priced when compared with other products available for lightweight fill construction (expanded clay, EPS blocks, etc.) and also that performs better that other lightweight aggregates as backfill in seismic conditions (Xiao et al. 2013).

Despite these benefits TDA remains relatively marginal as a recycling outlet for waste tires (ETRMA 2016; RMA 2015; JATMA 2016). Two reasons of technical nature may explain this situation. The first one is related to environmental concerns. Some 20 years ago the initially fast development of TDA fills in the USA was abruptly halted after several incidents of self-combustion were observed. In these incidents TDA fills self-ignited after construction

Can. Geotech. J. Downloaded from www.nrcresearchpress.com by UNIVERSITAT POLITECNICA DE CATALUNYA on 04/03/18
For personal use only. This Just-IN manuscript is the accepted manuscript prior to copy editing and page composition. It may differ from the final official version of record.

without any clear external cause. Careful study and comparison of these cases with the vast majority of successful examples already available at the time resulted in empirical design guidelines (Ad Hoc Civil Engineering Committee 2002; ASTM 2008) that, when followed, have avoided any repetition of the problem (Tandon et al. 2007). Later research (Sellasie et al. 2004; Wappett and Zornberg 2006) further clarified the cause of this problem (exposed steel oxidation), providing also a methodology for analysis and quantification (Arroyo et al. 2011). Other potential environmental problems, related to water quality, are also easily avoided as shown by several studies (Humphrey and Swett 2006; Hennebert et al. 2014). It may be then concluded that environmental concerns should not be anymore an obstacle for the technique.

A second possible obstacle may be the relative unfamiliarity of TDA as construction material. TDA is a peculiar granular material in which, unlike soils, grain deformation plays a significant role. TDA grains have also elongated shapes that may deform in bending: most of this deformation is recoverable. It is then not surprising that elastic properties of TDA have received particular attention. Although secant modulus approximations are usefully applied (Ahn et al. 2015), numerical analyses can easily accommodate more elaborate and precise models. Proposals in this respect include non-linear elastic models (Lee et al. 1999; Meles et al. 2015) as well as anisotropic elastic models (Heimdahl and Drescher 1999; Jeremić et al. 2004). In principle a decision on which model is most appropriate for a particular application should be helped by comparison with laboratory testing. However, because of its large size it is difficult to test full-size TDA in the laboratory by means of conventional apparatus. Satisfactory results can be obtained using large scale apparatus (Strenk et al. 2007; Arroyo et al. 2008 and Yi et al. 2014) but these are not always readily available. Consequently a larger role than usual is played by field demonstration projects.

Indeed, well documented case histories of TDA applications are necessary to increase

Can. Geotech. J. Downloaded from www.nrcresearchpress.com by UNIVERSITAT POLITECNICA DE CATALUNYA on 04/03/18
For personal use only. This Just-IN manuscript is the accepted manuscript prior to copy editing and page composition. It may differ from the final official version of record.

confidence on the material and demonstrate its possibilities. There have been many documented applications in which TDA lightweight fill has been used as part of embankments on soft soils (Humphrey et al. 1998; Bosscher et al. 1997; Yoon et al. 2006), landslide repair (Ahn et al. 2015) or wall backfill (Lee et al. 1999; Xiao et al. 2013). However, one area of potential large scale TDA application which has not been previously documented is that of lightweight fill over tunnels, in which there is a potential for substantial savings in lining design. The study focus is on lining design under static actions, which is relevant for areas of low seismicity.

In what follows we first describe a recent field test in which TDA was used within the fill covering a newly built railway tunnel. Field measurements are analyzed to calibrate a 3D numerical model of the tunnel which is later used to explore the influence of alternative fill configurations and constitutive descriptions of the TDA. Finally some conclusions and recommendations for the use of TDA in this type of application are given.

Case History

General description

A cut-and-cover tunnel located within the high speed train corridor between Madrid and La Coruña (NW Spain) was selected for a demonstration project. The tunnel was located away from inhabited areas, so vibration was not an issue. Hence the focus of the project was on lining relief derived from the lightweight property of TDA and not in other potentially interesting applications for railway tunnels, such as vibration damping (well documented, for instance, in Cheng, 2016). To observe lining relief effects TDA fill needs to be placed above the tunnel. The final TDA configuration selected for the project was conditioned by logistic and administrative reasons. Indeed, the owner required strict adherence to current ASTM guidelines, and would not countenance a reduction in the lining originally designed before the

Can. Geotech. J. Downloaded from www.nrcresearchpress.com by UNIVERSITAT POLITECNICA DE CATALUNYA on 04/03/18
For personal use only. This Just-IN manuscript is the accepted manuscript prior to copy editing and page composition. It may differ from the final official version of record.

demonstration took place.

The tunnel cross section is shown in Figure 1. The tunnel was cast-in-situ, partly excavating the alternating layers of sandstones and siltstones present on site to attain grade. The arch section was supported on the natural ground and then covered by fill. Rock quality in the lower third of the section was good and the excavation was there restricted to that strictly necessary to cast the arch; the narrow excavated section behind the arch was then backfilled with lean concrete. Except at the tunnel portals, were some rockfill protection was arranged, the covering fill was zoned as follows

- Granular fill 1: Placed around the tunnel up to 1.5 m above its crown. It is a relatively high quality granular fill in agreement with the general specifications of the railway infrastructure operator (ADIF 2001).
- TDA layer: The TDA was specified as Type B TDA as per ASTM D6270 (2008). This is a material with maximum size of 450 mm and less than 1% below 4.75 mm (the gradation is given in Table 1), tightly controlled to limit exposed steel contents and the presence of contaminants. The layer was 70 m long, 17 m wide (being symmetrical about the tunnel axis), and 2 m thick, as shown in Figure 2 and Figure 3. The TDA layer was placed 1 m above the tunnel crown. To maintain separation of granular fill and TDA, the TDA was wrapped in a geotextile (non-woven, needle-punched polypropylene geotextile of 200 g/m^2).
- Granular fill 2: Granular fill placed everywhere above 1.5 m of the tunnel crown, except where substituted by the TDA layer. It is a medium quality fill, in agreement with the general specifications of the railway infrastructure operator (ADIF, 2001).

Monitoring was arranged on five cross-sections of the tunnel (Figure 2). All of them included topographic targets within the tunnel section. On sections S1, S2 and S3 additional devices were installed (Figure 3) including settlement platforms, earth pressure cells on the external

Can. Geotech. J. Downloaded from www.nrcresearchpress.com by UNIVERSITAT POLITECNICA DE CATALUNYA on 04/03/18
For personal use only. This Just-IN manuscript is the accepted manuscript prior to copy editing and page composition. It may differ from the final official version of record.

face of the tunnel wall and piezometers (some 3 m away from the earth pressure cells). On the two sections with TDA (S1 and S3) thermistors were also included. As shown in Figure 2, the main control sections (S1, S2 and S3) are all located where the height of the fill attains its maximum, at 11 m above the tunnel crown. While sections S1 and S3 include the TDA layer, section S2 does not, thus facilitating comparisons. Reading of each instrument started as they were placed and was continued after construction, up to nine months after the end of construction.

In order to avoid possible confusion related to the following exposed and commented values, from now on data from monitoring devices will be named as "measured values" while those from numerical calculations will be named as "predicted values" or "calculated values".

Observations during construction

Construction of the fill started on the 10/06/2014. The fill was raised maintaining equal heights on both sides of the tunnel. Settlement above the fill was not an issue in this application and the TDA material was simply extended using bulldozers, in layers 40±10 cm thick, without further compaction (Figure 4). Figure 5 shows the evolution of the height of the fill above the TDA layer at the main control sections S1, S2 and S3. That final filling phase took approximately 3 weeks, ending on 22/07/2014, after which date no more significant construction activity took place.

The longest measurement records are those of the topographic targets inside the tunnel. Figure 6 presents the settlement readings at the crown for the five monitoring sections. The records stabilize almost immediately after the fill construction stops (22/07/2014). A much reduced rate of displacement is visible during the first week of July: this coincides with the moment in which the TDA layer was extended. The main effect visible in the graph is that due to the variable fill height alongside the tunnel. Sections 0 and 4, which are closer to the tunnel portals and have smaller fill heights (3 m and 3.5 m above crown, respectively) show

Can. Geotech. J. Downloaded from www.nrcresearchpress.com by UNIVERSITAT POLITECNICA DE CATALUNYA on 04/03/18
For personal use only. This Just-IN manuscript is the accepted manuscript prior to copy editing and page composition. It may differ from the final official version of record.

smaller settlements. This is also visible in Figure 7, where the final section displacements in all tunnel control sections are plotted in polar coordinates co-centric with the section upper arch (see Figure 1). It is only on sections 1 to 3, where the fill is at full height (11 m to 11.5 m above the crown), that the tunnel arch shows a significant counterflexure.

Piezometric readings always indicated a water table located at the original soil substrate. The performance of the earth pressure cells located at the tunnel outer wall was disappointing. Readings during fill construction were unsuccessful so only initial readings (with fill height 4-5 m above the cells) and readings well after end of construction are available (Table 2). Moreover, the cell at section 3 failed after initial reading and that at section S1 showed clear signs of poor performance, with initial readings well below the other two and poor sensitivity to fill height increase. The most likely cause for the failure of cell at section 3 is cable damaged due to the fill settlement. As for the cell in section 1 the temperature record of the cell indicates a significant decrease of temperature after installation. It is then likely that the poor conformance observed may be due to thermal-induced cell shrinkage. Future installations of cells should consider and prevent these shortcomings, by increasing the protection and slack of the cables and avoiding the installation of cells just after being exposed for a long time to the sun, especially in summer.

Despite those shortcomings, the final pressure measured at section S2 (123 kPa) is close to what may be expected given the fill densities and friction (Table 5). Indeed, assuming at-rest conditions apply on the contact with the tunnel wall, we have

$$\sigma_h = \sigma_h^{'} = \sigma_v^{'} \cdot K_0 \cong (8{\cdot}18 + 2{\cdot}6.4 + 7.5{\cdot}19) \cdot (1 - \sin 35) = 128 \text{ kPa}$$

Final readings of the settlement platforms are presented in Table 3. Settlements below the TDA layer in section 1 are clearly anomalous, indicating large deformation in the fill layer that is not present in other sections, likely indicative of some operational problem during construction. From the measurements obtained at the settlement platforms the evolution of

Can. Geotech. J. Downloaded from www.nrcresearchpress.com by UNIVERSITAT POLITECNICA DE CATALUNYA on 04/03/18
For personal use only. This Just-IN manuscript is the accepted manuscript prior to copy editing and page composition. It may differ from the final official version of record.

the in-between layer thickness may be obtained (Figure 8). Clearly the amount of layer shortening in the TDA cases (sections 1 and 2) is far higher than that observed in the granular fill. In all cases, the movements stabilize soon after the end of the fill construction. The observed compression of the TDA layer was employed to obtain a secant modulus $E_{in\text{-}situ}$, as

$$(1)\quad E_{in\_situ} \cong \frac{\gamma_{fill2} \cdot H_{fill2}}{\Delta s} \cdot H_{material}$$

Where Δs, is the differential settlement, as recorded between the upper and lower plates of each section, H_{fill2} is the height of the fill 2 over the upper plate and $H_{material}$ is the thickness of the layer between plates 1 and 2 (TDA in sections 1 and 2, and granular fill 2 in section 3). Results from these estimations are indicated in Table 4. The observed secant modulus at sections with TDA is much smaller than that at the section with granular fill.

Temperature readings inside the TDA layer showed no build up in temperature after placement, quickly converging towards the values recorded outside the TDA in the temperature transducers located within earth cells and piezometers (around 25 ºC).

Numerical Analyses

General model features

For the analysis of the tunnel a three dimensional finite difference model was developed using the commercial code FLAC3D. The model includes approximately 183,000 elements and 196,000 nodes; its general layout is shown in Figure 9. Boundary conditions are:

- 'x' displacements impeded in lateral borders.
- 'y' displacements impeded in frontal and back borders.
- All displacements impeded at the bottom of the mesh.

Sensitivity analyses on the numerical model were employed to check that the distances to the boundaries selected in the model were enough to avoid boundary effects on the results.

Can. Geotech. J. Downloaded from www.nrcresearchpress.com by UNIVERSITAT POLITECNICA DE CATALUNYA on 04/03/18
For personal use only. This Just-IN manuscript is the accepted manuscript prior to copy editing and page composition. It may differ from the final official version of record.

Initial conditions represent the situation existing after the excavation of the original soil, and before building the tunnel lining. The initial in situ stresses for this situation are estimated by means of the above mentioned boundary conditions and the mechanical properties of the substrate shown in Table 5. The water table is located close to the substrate.

The model calculation closely follows the sequence of field operations, the phases considered in the analysis are:

- Phase 0: the *in situ* stress state of the ground is obtained.
- Phase 1: Activation of the tunnel lining and the lean concrete fill.
- Phase 2: Activation of fill 1 and rockfill protection at tunnel entrances.
- Phase 3: Activation of TDA layer.
- Phase 4: Activation of fill 2 layer up to the top level of TDA layer.
- Phase 5: The remaining fill 2 is activated up to its final elevation

Material properties

Apart from the TDA, five different materials are included in the model: substrate, rockfill, two different granular fills and concrete. A Mohr-Coulomb elasto-plastic constitutive model has been used for all of them, except for the concrete, for which an elastic model was used. The properties selected for these materials were based on the site investigation and construction records (Table 5).

For the TDA layer three different material models were used. The models differ in the elastic idealizations employed, since all of them can be described as elasto-plastic models with a Mohr Coulomb envelope. The first elastic idealization was the simplest: isotropic linear eleasticity. In the second case the linearity assumption was relaxed, using instead a model described by Meles et al. (2015). Based on large scale oedometric testing Meles et al. (2015) proposed several nonlinear stress-strain expressions for different TDA types, all of them with the form

Can. Geotech. J. Downloaded from www.nrcresearchpress.com by UNIVERSITAT POLITECNICA DE CATALUNYA on 04/03/18
For personal use only. This Just-IN manuscript is the accepted manuscript prior to copy editing and page composition. It may differ from the final official version of record.

(2) $\varepsilon = \frac{\sigma}{a + b \cdot \sigma}$

Where σ = axial stress (kPa); and ε = axial strain (%). Finally, the third model considered is the elastic cross-anisotropic model described by Jeremic et al. (2004).

The parameters defining the Mohr Coulomb envelope were estimated from the literature (Yang et al. 2001; Arroyo et al. 2008; Humphrey 2008). The in situ density was estimated from the site records. The observed $E_{in\text{-}situ}$ was employed to calibrate parameters of the different models as follows.

1. For the elastic isotropic model $E \approx E_{in\text{-}situ} = 630$ kPa
2. For the non-linear model, equation (2) was applied. A value of $b = 2.65$ was selected in agreement with the values proposed by Meles et al. (2015) for ASTM type B (TDA used for embankment fill) PLTT (passengers and light truck tires). The value of parameter *a* was adjusted to fit the field data (σ = 144 kPa, $E_{in\text{-}situ}$ = 630 kPa $\Rightarrow \varepsilon$ = 0.2286). This adjusted parameter value results in a somewhat more rigid response that that originally proposed. Finally, the expression introduced in the numerical model to compute a non-linear elastic modulus was

   (3) $\varepsilon = \frac{\sigma}{248 + 2.65 \cdot \sigma} \Rightarrow E = 248 + 2.65 \cdot \sigma$

3. When calibrating the anisotropic model, Jeremic et al. (2004) obtained the following values:

   E_{11} = 5000 kPa, E_{33} = 3330 kPa, $\nu_{12} = 0.11$, $\nu_{13} = 0.37$, $\nu_{31} = 0.11$

   Where E_{11} (= E_{22}) and E_{33} are the in-plane and out-of-plane Young moduli, respectively. ν_{12} (=ν_{21}) is the in-plane Poisson's ratio; ν_{31} and ν_{13} are the out-of-plane Poisson's ratio.

   The observed in situ secant modulus value was used to calibrate the relevant out-of-plane modulus

Can. Geotech. J. Downloaded from www.nrcresearchpress.com by UNIVERSITAT POLITECNICA DE CATALUNYA on 04/03/18
For personal use only. This Just-IN manuscript is the accepted manuscript prior to copy editing and page composition. It may differ from the final official version of record.

$E_{33} = E_{in\text{-}situ} = 630$ kPa

It was then assumed that the same moduli ratios obtained in the laboratory were valid in the field. Thus, Poisson ratios were the same as in Jeremic et al. (2004) and the in-plane modulus value was then selected to maintain the ratio between the E_{11} and E_{33} moduli obtained in the laboratory, giving E_{11} (= E_{22}) = 946 kPa. Thus, the material behavior is expected to be somewhat more rigid than that corresponding to the linear elastic model, where $E_{11} = E_{22} = E_{33} = 630$ kPa.

The calibrated parameters for TDA in all cases are collected in Table 6.

Base case: effect of TDA material description

In this section analyses are presented in which the geometry of the numerical model is fixed, always representing the geometry built for the field test. Three computations are carried out, one for each of the different material models calibrated for the TDA. Figure 10 represents the final longitudinal settlement profiles above the TDA layer obtained with the three different mechanical models, alongside the measurements of the settlement plates. The profiles obtained with the linear isotropic and the non-linear isotropic models are very similar, due to the similar computed elastic moduli these models employ. Interestingly, the anisotropic model response appears more rigid, reducing settlement estimate by 22%. The anisotropic model behaves more rigidly because the out-of-plane modulus is higher than the in-plane modulus value that is also used by the linear isotropic and the non-linear isotropic models. Observed settlements at sections 2 and 3 are well captured, not so the anomalous readings of section 1. It is likely that this device was moved accidentally by the construction machinery, as the settlement registered just above the 1.5 m-thick granular layer below the TDA (33 cm, see Table 3) appears out of range for well compacted granular soil.

Displacements of the lining in polar coordinates co-centric with the section upper arch, are presented in Figure 11. The simulated results compare well with measured displacements

Can. Geotech. J. Downloaded from www.nrcresearchpress.com by UNIVERSITAT POLITECNICA DE CATALUNYA on 04/03/18
For personal use only. This Just-IN manuscript is the accepted manuscript prior to copy editing and page composition. It may differ from the final official version of record.

from the topographic targets, especially in the left side of the section. Values in the right side fit a little worse because of the surprisingly lower movements measured in this side. As the cross section of the fill (Figure 2) has more weight in its right side than in the left side, no satisfactory explanation has been found for these lower values apart from possible measurement error. Differences between values of convergences when employing different constitutive models for the TDA material are irrelevant, always smaller than 3%, and may be caused by the different final elastic moduli of the TDA material computed from the different constitutive models. The rigidity of this layer slightly influences stress transfer from the upper part of the fill towards the tunnel liner.

Finally, Figure 12 shows the bending moments in the lining in polar coordinates. Results from a computation in which no TDA layer is present in the model are also included for reference. It appears that the presence of the TDA layer reduced a little (15%) the magnitude of bending moments in the section. Again, the effect on this result of the different TDA constitutive descriptions is almost negligible.

Study of alternative TDA configurations

The single TDA layer applied in the field test reduced the vertical stress at the tunnel crown level by some 15%, hence the potential improvement effect was limited. It is interesting to explore what effects might have followed from alternative TDA configurations. To do so, two new models were created with different geometrical configurations of the TDA material. For both configurations three analyses were carried out, to investigate the effect of the TDA elastic material model (isotropic, anisotropic and non-linear isotropic) also in these cases. Results from a calculation without any TDA are also included for comparison purposes.

Figure 13 illustrates transverse sections of the following two models:

- 2 TDA Layers. This configuration can be seen as a thicker version of what was built, at the upper limit of class II TDA fills as per ASTM D 6270-08. The TDA layers are

Can. Geotech. J. Downloaded from www.nrcresearchpress.com by UNIVERSITAT POLITECNICA DE CATALUNYA on 04/03/18
For personal use only. This Just-IN manuscript is the accepted manuscript prior to copy editing and page composition. It may differ from the final official version of record.

65 m long, 17 m wide (being symmetrical about the tunnel axis) and 3 m thick. The lower one is placed 1 m above the tunnel crown and the upper one is separated 1 m from the previous.

- Surrounding TDA. In this configuration the same volume of TDA as in the previous case is disposed in a single layer surrounding the tunnel arch. This disposition goes somewhat beyond ASTM D 6270-08, because it may ease free access to air into the TDA fills. However, detailed analyses by Arroyo et al (2011) have shown that a TDA fill in which exposed steel is limited following other ASTM D 6270-08 provisions will generate very little heat, and that allowing air circulation in such fill actually reduces the eventual temperature rise.

Figure 14 shows the longitudinal settlement profiles at the embankment surface obtained for the different calculations. The 2-layer configuration results in less surface settlement than the surrounding configuration, for all material models. This is reasonable since stresses acting on the TDA are higher for the surrounding configuration. When comparing different constitutive models for the TDA material, the linear anisotropic approach predicts lower settlements than the linear isotropic model does (around 18%). The maximum settlements are predicted by the non-linear isotropic model (about 9% higher than those calculated with the linear isotropic model).

The picture is very different when attention is focused on the buried structure. Estimated final tunnel convergences for the six cases analyzed are presented in Figure 15. Computed convergences show very little sensitivity to the different constitutive models for the TDA material. In all cases, convergences decrease with respect to those calculated without TDA. On average, convergence reduction is larger (around 17%) for the surrounding TDA configuration than for the 2-layer one (some 10%). However, it should be noted that predicted settlements at the crown are almost identical for the two configurations and that the

Can. Geotech. J. Downloaded from www.nrcresearchpress.com by UNIVERSITAT POLITECNICA DE CATALUNYA on 04/03/18
For personal use only. This Just-IN manuscript is the accepted manuscript prior to copy editing and page composition. It may differ from the final official version of record.

difference between the two configurations is mostly due to the lesser inward displacement observed on the tunnel sides for the surrounding configuration.

The convergence pattern just discussed can be related to the changes in stress distribution that result from the different TDA configurations (Figure 16). The presence of granular fill around the tunnel in the 2-layer configuration there results in a more homogenous state of stress around the lining. On the other hand, in the surrounding configuration the tunnel crown acts as a hard point, concentrating stress from the granular fill above the TDA and discharging the tunnel sides.

Finally, Figure 17 shows the corresponding bending moment envelopes. The effect of TDA configuration is remarkable. TDA disposed in the two-layer configuration significantly reduced positive bending moments (e.g. by 60% at the tunnel crown) without increasing negative moments (indeed reducing them almost everywhere). This beneficial effect for the structure is not observed for the surrounding configuration, inducing bending moments very similar to those calculated without TDA. This relatively poor performance of the surrounding TDA configuration is due to the highly asymmetric stress distribution around the lining that induces. The effect of the different constitutive models for the TDA material in this respect is, again, almost negligible.

Conclusions

From the case history data and subsequent analysis it may be concluded that:

1. Construction of TDA fills above cut-and-cover tunnels can be achieved successfully by similar means as those employed for other TDA fill applications, like embankments on soft soils.
2. When numerical analyses are used to estimate settlements and tunnel lining loads, the elastic constitutive model chosen is secondary as long as it is calibrated with field

Can. Geotech. J. Downloaded from www.nrcresearchpress.com by UNIVERSITAT POLITECNICA DE CATALUNYA on 04/03/18
For personal use only. This Just-IN manuscript is the accepted manuscript prior to copy editing and page composition. It may differ from the final official version of record.

measurements. In absence of such measurements, the model proposed by Meles et al. (2015) appears reasonably conservative.

3. If the main objective sought with the introduction of the TDA fill is to reduce static loads on the tunnel lining, TDA layered fills above the crown are more beneficial than fill configurations that closely surround the tunnel.

The study presented has focused on the benefits that may be derived from the lightweight property of TDA for tunnel design under static loads. Further studies are required to document the possible added benefits that may be observed under dynamic loading due to the high damping property that characterizes TDA.

The conclusions above are limited to tunnel geometries similar to that of the case analyzed. Extending them to different tunnel sections and / or foundation conditions would require new analyses. Despite that it is hoped that the case here illustrated will encourage further use of TDA fills above cut-and-cover tunnels, a good recycling outlet for an inconvenient bulky residue.

Acknowledgment

The authors gratefully acknowledge to the *Centro de Desarrollo Tecnológico Industrial (CDTI)*, dependent of the Spanish *Ministerio de Economía y Competitividad* for funding this research work, which is included in the project entitled "*Application of industrial waste paper and used tires for the construction of ecological lightened embankments and other construction materials*". They also acknowledge to the company Sacyr and the *Laboratorio de Geotecnia del CEDEX* dependent of the *Ministerio de Fomento* for their helpful comments and ideas in developing the test site.

Can. Geotech. J. Downloaded from www.nrcresearchpress.com by UNIVERSITAT POLITECNICA DE CATALUNYA on 04/03/18
For personal use only. This Just-IN manuscript is the accepted manuscript prior to copy editing and page composition. It may differ from the final official version of record.

References

ASTM (American Society of Civil Engineers). 2008. Standard Practice for Use of Scrap Tires in Civil Engineering Applications. ASTM D6270.

Ahn, I.S., Cheng, L., Fox, P.J., Wright, J., Patenaude, S., and Fujii, B. 2014. Material Properties of Large-Size Tire Derived Aggregate for Civil Engineering Applications. Journal of Materials in Civil Engineering, **27**(9): 04014258.

Arroyo, M., Estaire, J., Sanmartín, I., and Lloret, A. 2008. Size effect on TDA mechanical properties. International workshop on Scrap Derived Geomaterials. Yokosuka, Japan.

Arroyo, M., San Martín, I., Olivella, S., and Saaltink M.W. 2011. Evaluation of self-combustion in tire derived aggregate fills. Waste management, **31**(9-10): 2133-2141.

Bosscher, P., Edil, T., and Kuraoka, S. 1997. Design of Highway Embankments Using Tire Chips. J. Geotech. Geoenviron. Eng., 10.1061/(ASCE)1090-0241(1997)123:4(295), 295-304.

Brunet, S., de la Llera, J.C., and Kausel, E. 2016. Non-linear modeling of seismic isolation systems made of recycled tire-rubber. Soil Dynamics and Earthquake Engineering, 85, 134-145.

Cheng, D. 2016. Usage Guide. Tire derived aggregate (TDA), Report DRRR 2016-01545, California Department of Resources Recycling and Recovery (CalRecycle).

Eldin, N.N., and Senouci, A. 1992. Use of scrap tires in road construction. Journal of Construction Engineering and Management, 118, 561-576.

ETRMA, European Tyre & Rubber Manufacturers Association. 2016. End-of-life tyre report 2015, Available from http://www.etrma.org/

Heimdahl, T.C., and Drescher, A. 1999. Elastic anisotropy of tire shreds. Journal of Geotechnical and Geoenvironmental Engineering, **125**(5): 383-389.

Can. Geotech. J. Downloaded from www.nrcresearchpress.com by UNIVERSITAT POLITECNICA DE CATALUNYA on 04/03/18
For personal use only. This Just-IN manuscript is the accepted manuscript prior to copy editing and page composition. It may differ from the final official version of record.

Hennebert, P., Lambert, S., Fouillen, F., and Charrasse, B. 2014. Assessing the environmental impact of shredded tires as embankment fill material. Canadian Geotechnical Journal, **51**(5): 469-478.

Humphrey, N.D. 2008. Tire shreds as lightweight fill for embankments and retaining walls. Proc., International workshop on Scrap Derived Geomaterials. Fokuoka, Japan.

Humphrey, D.N., and Swett, M. 2006. Literature review of the water quality effects of tire derived aggregate and rubber modified asphalt pavement. Dept. of Civil and Environmental Engineering, Univ. of Maine, Orono, ME.

Jaky, J. 1948. Pressure in silos. Proc., 2nd International Conference on Soil Mechanics and Foundation Engineering, 103-107.

JATMA, Japan automobile tyre manufacturers association. 2016. Tyre industry of Japan. 2016. Available from: <http://www.jatma.or.jp>.

Jeremić, B., Putnam, J., Sett, K., Humphrey, D., and Patenaude, S. 2004. Calibration of elastic-plastic material model for tire shreds. In Geotechnical Engineering for Transportation Projects (pp. 760-767).

Lee, J.H., Salgado, R., Bernal, A., and Lovell, C.W. 1999. Shredded tires and rubber-sand as lightweight backfill. Journal of Geotechnical and Geoenvironmental Engineering, **125**(2): 132-141.

Meles, D., Chan, D., Yi, Y., and Bayat, A. 2015. Finite-Element analysis of highway embankment made from Tire-Derived Aggregate. J. Mater. Civ. Eng., **28**(2).

RMA, Rubber manufacturers association. 2017. US Scrap tire management summary. Available from <http://www.rma.org/scrap_tires/>.

Strenk, P.M., Wartman, J., Grubb, D.G., Humphrey, D.N., and Natale, M.F. 2007. Variability and scale-dependency of tire-derived aggregate. Journal of materials in civil engineering, **19**(3): 233-241.

Can. Geotech. J. Downloaded from www.nrcresearchpress.com by UNIVERSITAT POLITECNICA DE CATALUNYA on 04/03/18
For personal use only. This Just-IN manuscript is the accepted manuscript prior to copy editing and page composition. It may differ from the final official version of record.

Tandon, V., Velazco, D.A., Nazarian, S., and Picornell, M. 2007. Performance monitoring of embankments containing tire chips: case study. Journal of Performance of Constructed Facilities, 4, 207-214.

Yang, S., Kjartanson, B.H., and Lohnes, R.A. 2001. Structural performance of scrap tire culverts. Canadian Journal of Civil Engineering, 28, 179-189.

Yi, Y., Meles, D., Nassiri, S., and Bayat, A. 2014. On the compressibility of tire-derived aggregate: comparison of results from laboratory and field tests. Canadian Geotechnical Journal, **52**(4): 442-458.

Yoon, S., Prezzi, M., Siddiki, N.Z., and Kim, B. 2006. Construction of a test embankment using a sand-tire shred mixture as fill material. Waste Management, 26, 1033-1044.

Xiao, M., Tehrani, F., and Zoghi, M. 2013 Seismic Responses of MSE Walls Using Accelerated Alternative Backfill Materials with Recycled Tire Shreds and Lightweight Expanded Aggregates, Report CA13-2416, State of California, Department of Transportation

Can. Geotech. J. Downloaded from www.nrcresearchpress.com by UNIVERSITAT POLITECNICA DE CATALUNYA on 04/03/18
For personal use only. This Just-IN manuscript is the accepted manuscript prior to copy editing and page composition. It may differ from the final official version of record.

Figure Captions

Figure 1. Tunnel cross section.

Figure 2. Longitudinal section of the tunnel. Location of the 5 monitoring sections.

Figure 3. Instrument layout at monitoring sections S1, S2 and S3.

Figure 4. Construction of the TDA layer above the tunnel crown.

Figure 5. Fill height above the TDA layer at the three main control sections S1, S2 and S3.

Figure 6. Vertical displacements at tunnel crown.

Figure 7. Final displacements of topographic targets inside the tunnel. Polar coordinates from the center of the section upper arch.

Figure 8. Vertical distance between settlement platforms (layer thickness) at monitoring sections.

Figure 9 Finite difference mesh. (a) Perspective at final stage (b) cross section (S3)

Figure 10 Effect of different constitutive models on the final longitudinal settlement profile just above the TDA and data from the settlement platforms.

Figure 11 Effect of different constitutive models on computed convergences and comparison with available data from the topographic targets. Section 3.

Figure 12 Effect of introducing one TDA layer on computed bending moments. Section 3.

Figure 13 Alternative configurations for the TDA material within the section.

Can. Geotech. J. Downloaded from www.nrcresearchpress.com by UNIVERSITAT POLITECNICA DE CATALUNYA on 04/03/18
For personal use only. This Just-IN manuscript is the accepted manuscript prior to copy editing and page composition. It may differ from the final official version of record.

Figure 14 Effect of both different constitutive models and different TDA distributions on surface settlements.

Figure 15 Tunnel lining final displacements. Polar coordinates co-centric with the section upper arch. Effect of alternative TDA distributions.

Figure 16 Non-linear isotropic model. Central section (80 m from the portals). Contour plots of minimum principal stress magnitude. Contour interval 100 kPa. Lightest color 0-100 kPa. Darkest color 600-700 kPa.

Figure 17 Effect of both different constitutive models and different TDA distributions on computed bending moments.

Can. Geotech. J. Downloaded from www.nrcresearchpress.com by UNIVERSITAT POLITECNICA DE CATALUNYA on 04/03/18
For personal use only. This Just-IN manuscript is the accepted manuscript prior to copy editing and page composition. It may differ from the final official version of record.

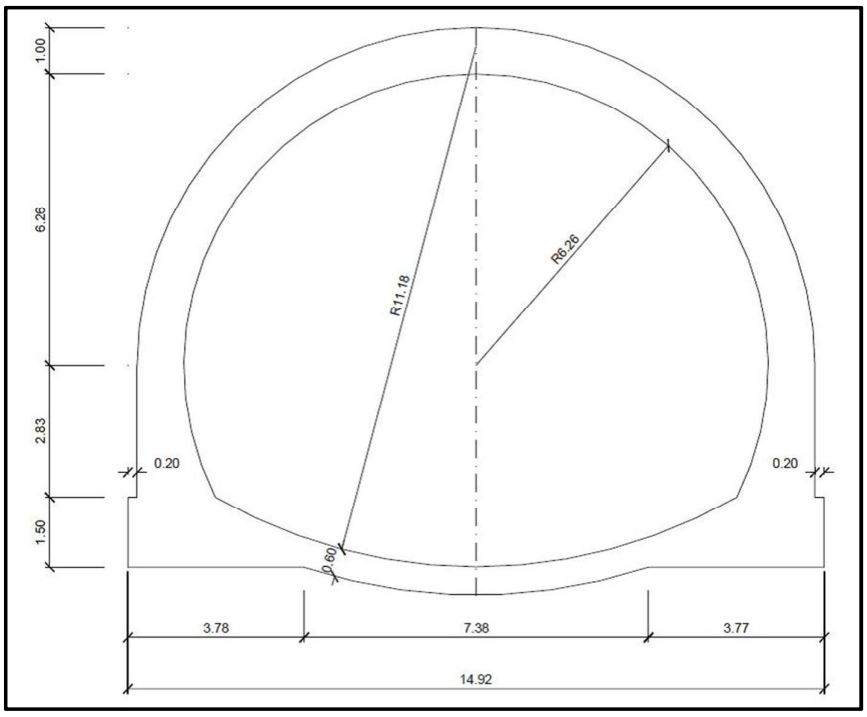

Figure 1. Tunnel cross section.

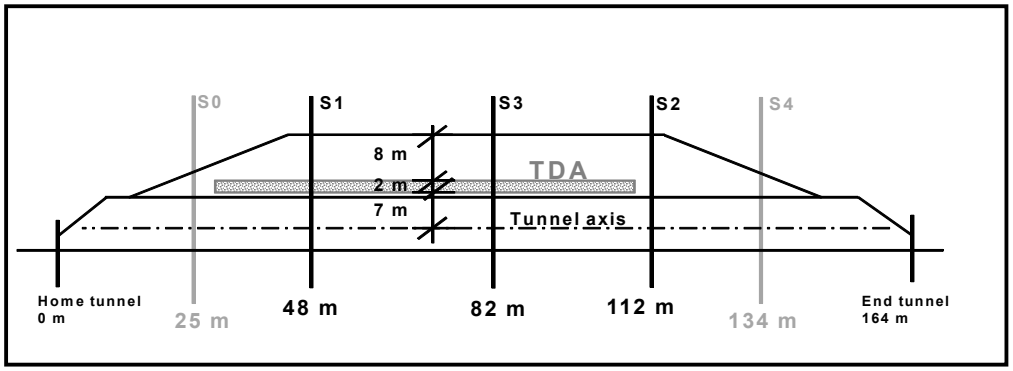

Figure 2. Longitudinal section of the tunnel. Location of the 5 monitoring sections.

Can. Geotech. J. Downloaded from www.nrcresearchpress.com by UNIVERSITAT POLITECNICA DE CATALUNYA on 04/03/18
For personal use only. This Just-IN manuscript is the accepted manuscript prior to copy editing and page composition. It may differ from the final official version of record.

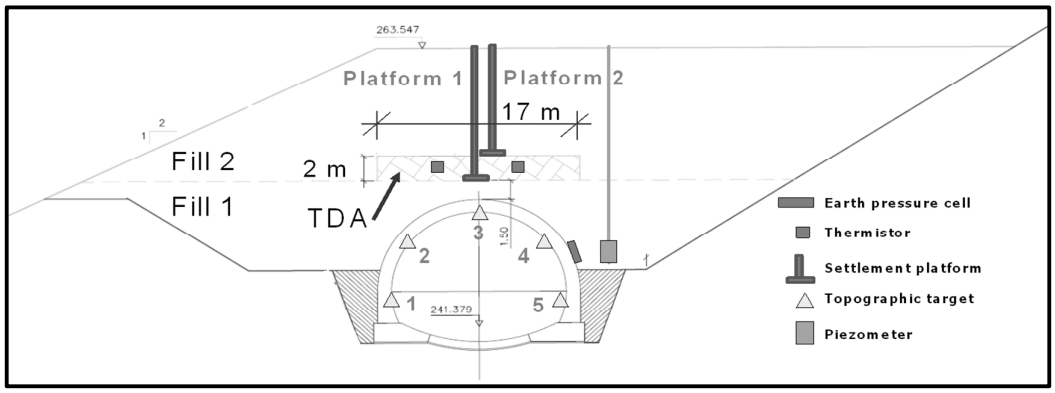

Figure 3. Instrument layout at monitoring sections S1, S2 and S3.

Figure 4. Construction of the TDA layer above the tunnel crown.

Can. Geotech. J. Downloaded from www.nrcresearchpress.com by UNIVERSITAT POLITECNICA DE CATALUNYA on 04/03/18
For personal use only. This Just-IN manuscript is the accepted manuscript prior to copy editing and page composition. It may differ from the final official version of record.

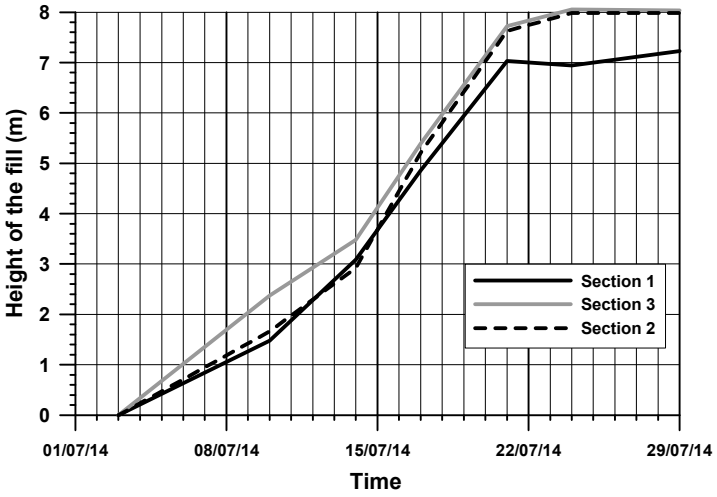

Figure 5. Fill height above the TDA layer at the three main control sections S1, S2 and S3.

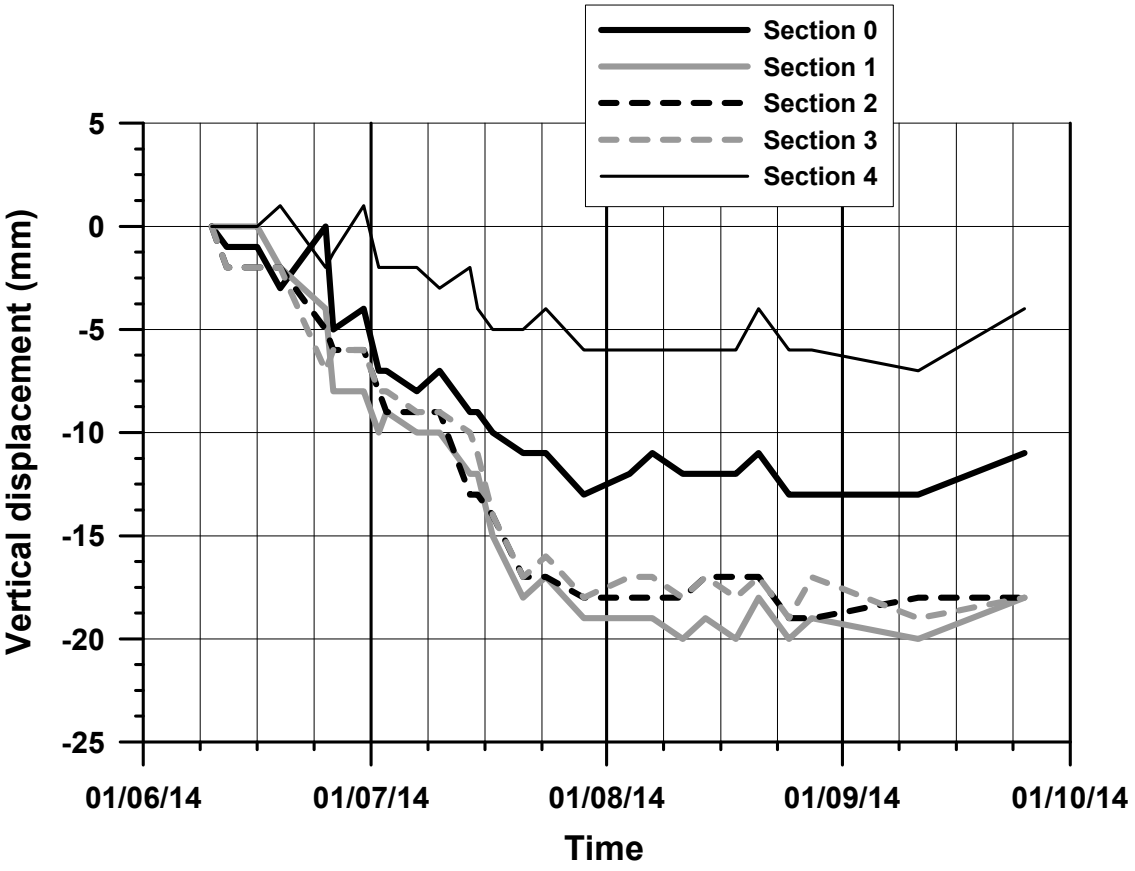

Figure 6. Vertical displacements at tunnel crown.

Can. Geotech. J. Downloaded from www.nrcresearchpress.com by UNIVERSITAT POLITECNICA DE CATALUNYA on 04/03/18
For personal use only. This Just-IN manuscript is the accepted manuscript prior to copy editing and page composition. It may differ from the final official version of record.

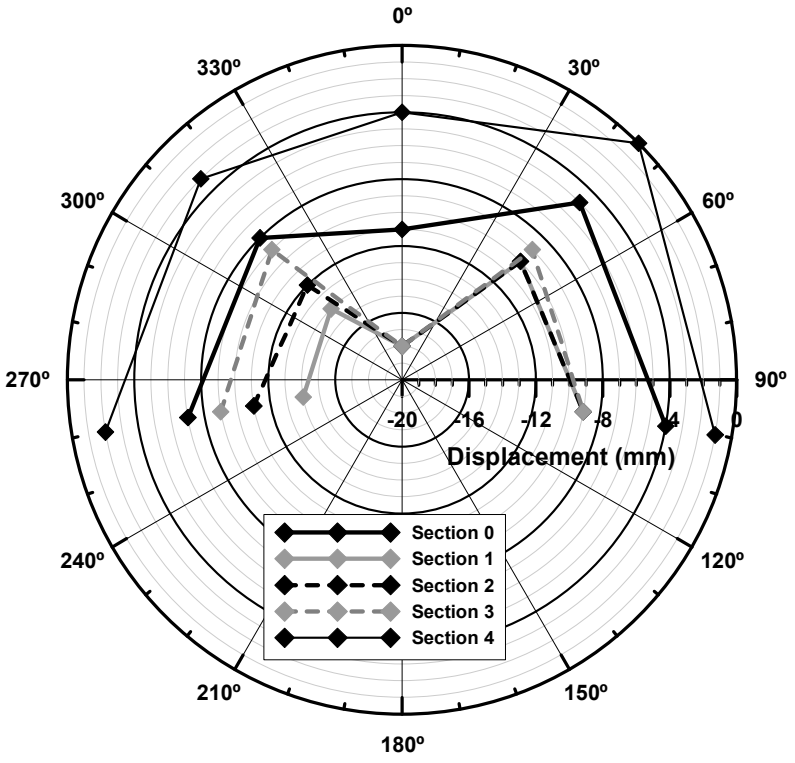

Figure 7. Final displacements of topographic targets inside the tunnel. Polar coordinates from the center of the section upper arch.

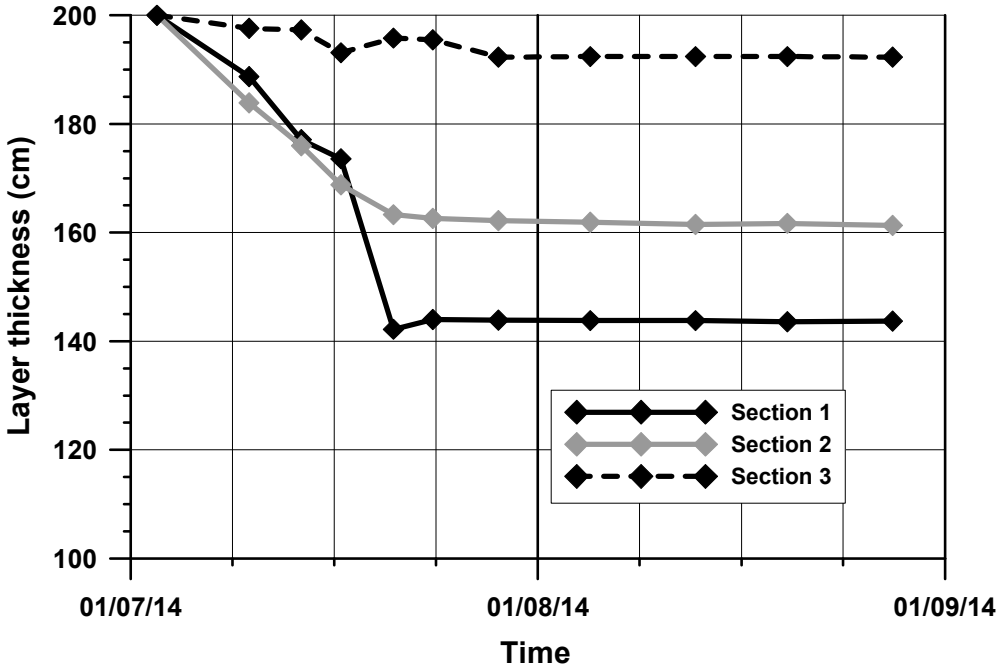

Figure 8. Vertical distance between settlement platforms (layer thickness) at monitoring sections.

Can. Geotech. J. Downloaded from www.nrcresearchpress.com by UNIVERSITAT POLITECNICA DE CATALUNYA on 04/03/18
For personal use only. This Just-IN manuscript is the accepted manuscript prior to copy editing and page composition. It may differ from the final official version of record.

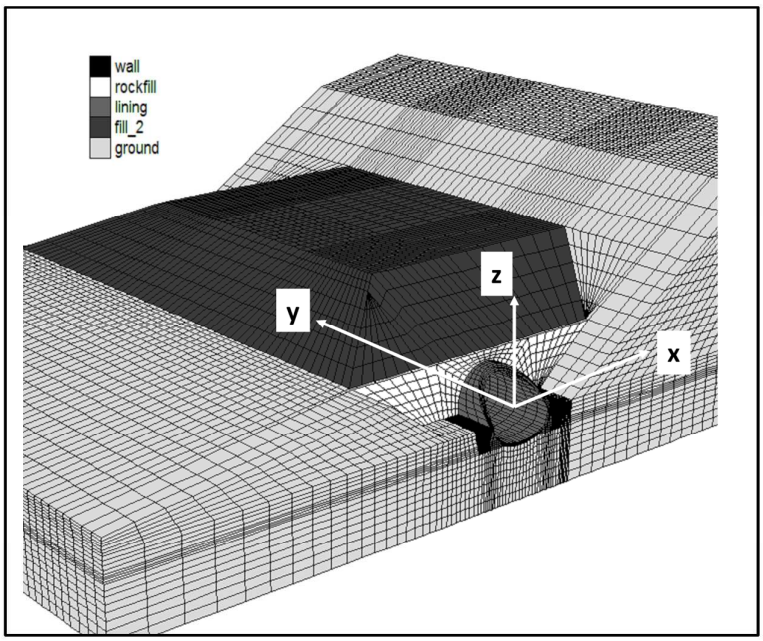

(a)

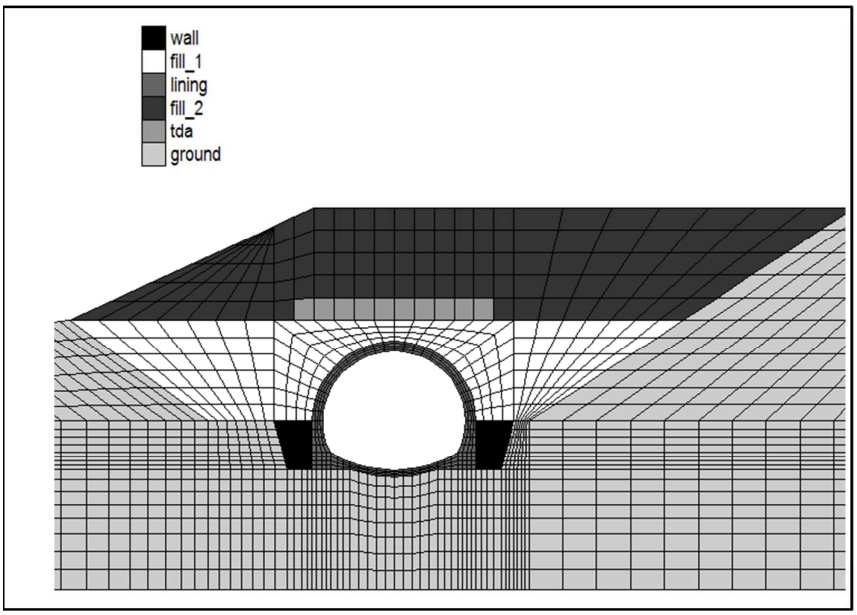

(b)

Figure 9 Finite difference mesh. (a) Perspective at final stage (b) cross section (S3)

Can. Geotech. J. Downloaded from www.nrcresearchpress.com by UNIVERSITAT POLITECNICA DE CATALUNYA on 04/03/18
For personal use only. This Just-IN manuscript is the accepted manuscript prior to copy editing and page composition. It may differ from the final official version of record.

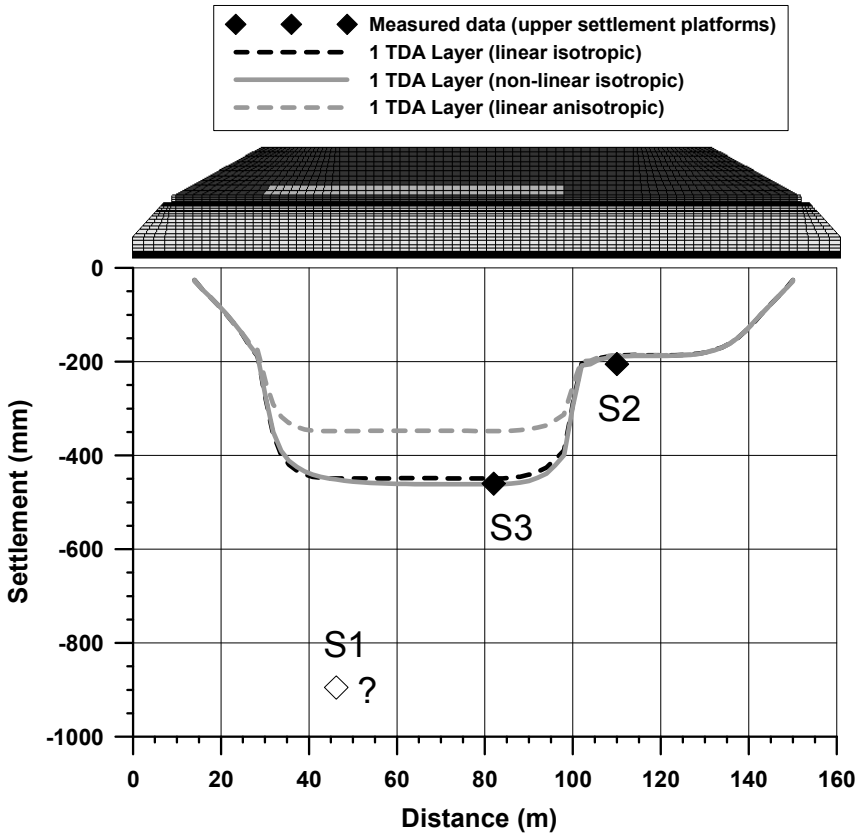

Figure 10 Effect of different constitutive models on the final longitudinal settlement profile just above the TDA and data from the settlement platforms.

Can. Geotech. J. Downloaded from www.nrcresearchpress.com by UNIVERSITAT POLITECNICA DE CATALUNYA on 04/03/18
For personal use only. This Just-IN manuscript is the accepted manuscript prior to copy editing and page composition. It may differ from the final official version of record.

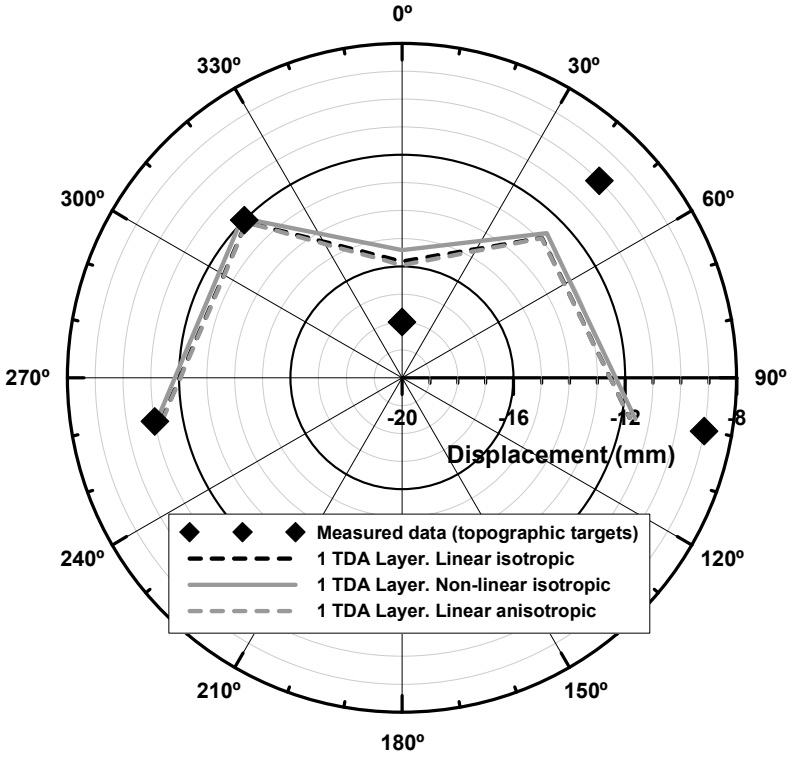

Figure 11 Effect of different constitutive models on computed convergences and comparison with available data from the topographic targets. Section 3.

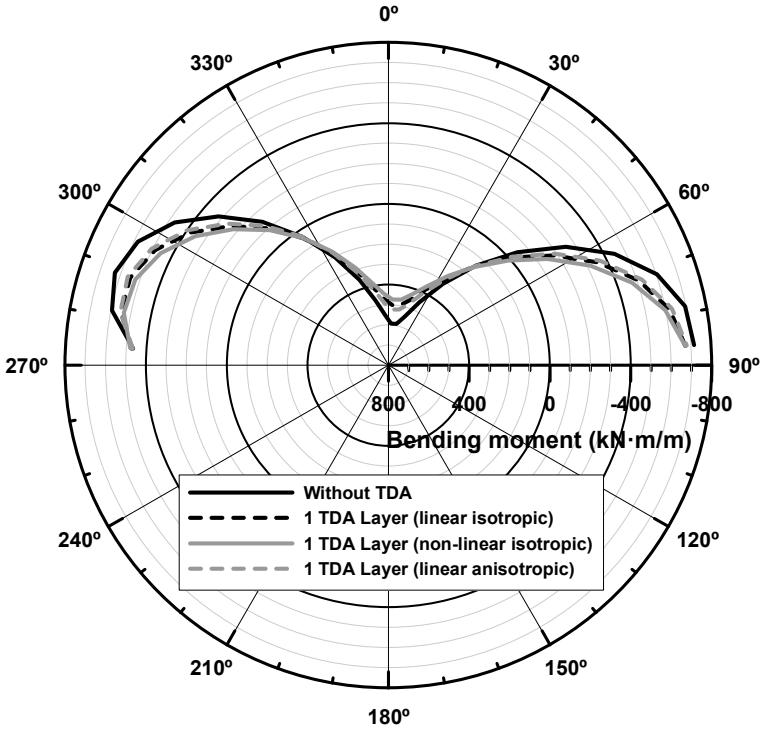

Figure 12 Effect of introducing one TDA layer on computed bending moments. Section 3.

Can. Geotech. J. Downloaded from www.nrcresearchpress.com by UNIVERSITAT POLITECNICA DE CATALUNYA on 04/03/18
For personal use only. This Just-IN manuscript is the accepted manuscript prior to copy editing and page composition. It may differ from the final official version of record.

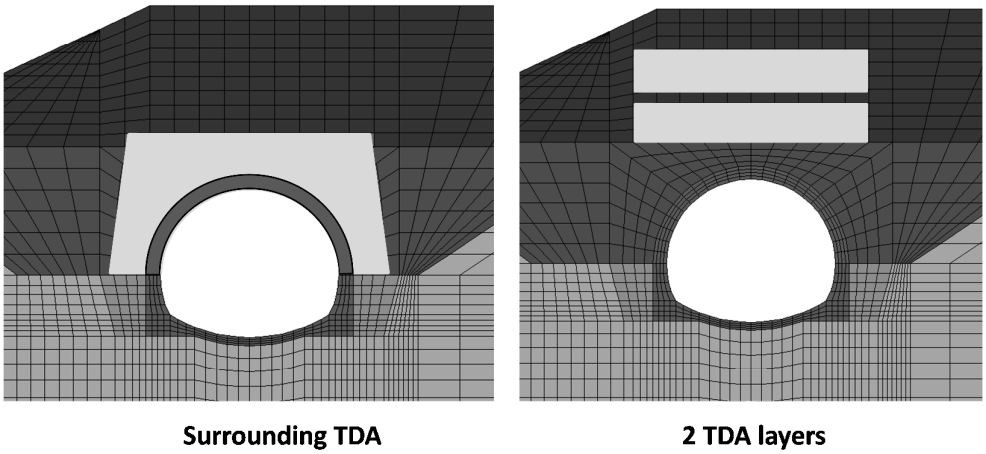

Figure 13 Alternative configurations for the TDA material within the section.

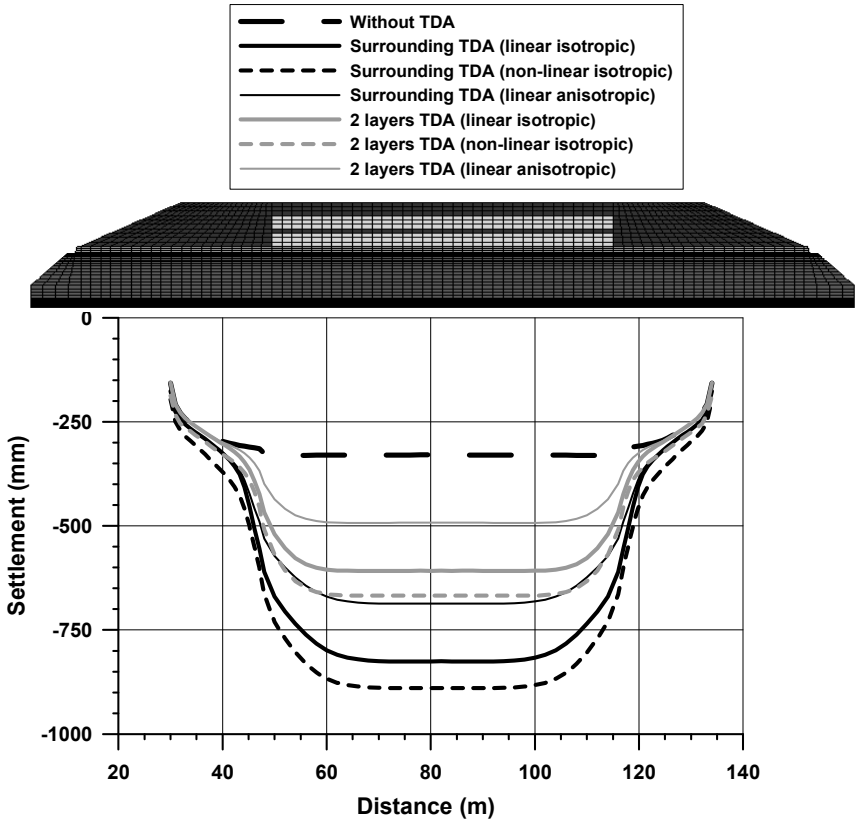

Figure 14 Effect of both different constitutive models and different TDA distributions on surface settlements.

Can. Geotech. J. Downloaded from www.nrcresearchpress.com by UNIVERSITAT POLITECNICA DE CATALUNYA on 04/03/18
For personal use only. This Just-IN manuscript is the accepted manuscript prior to copy editing and page composition. It may differ from the final official version of record.

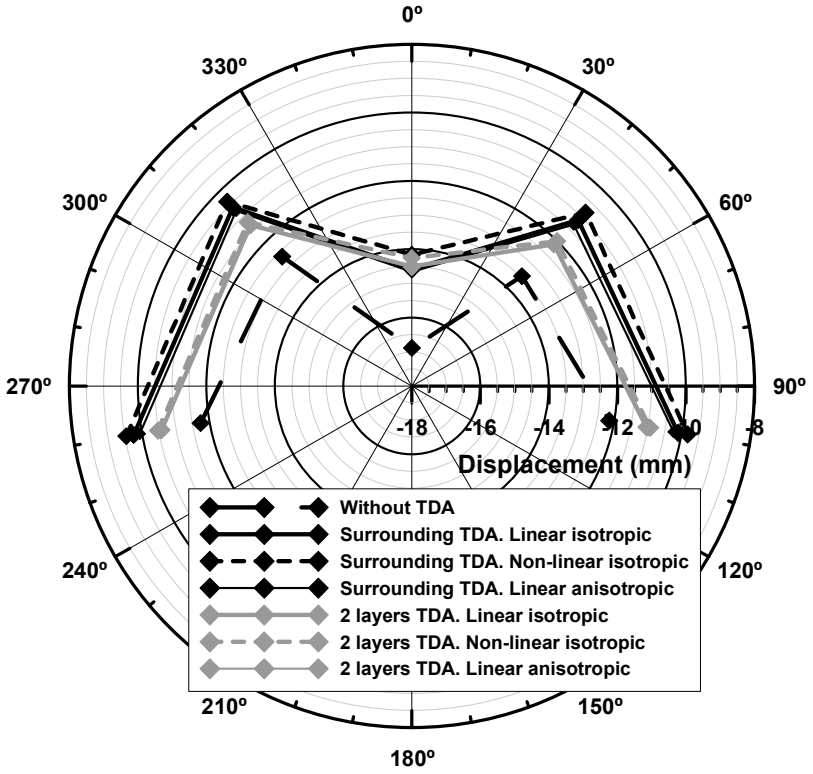

Figure 15 Tunnel lining final displacements. Polar coordinates co-centric with the section upper arch. Effect of alternative TDA distributions.

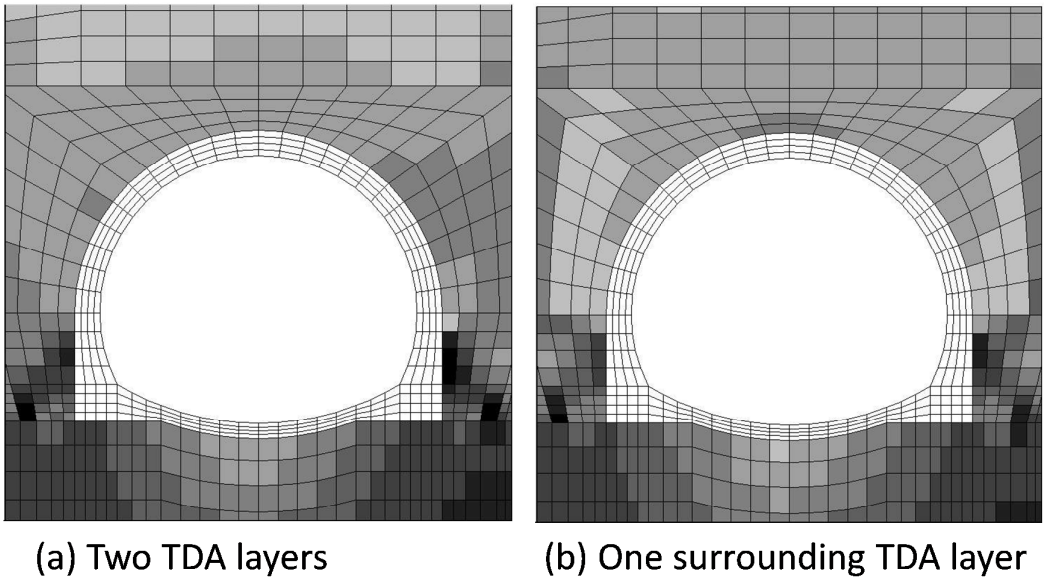

Figure 16 Non-linear isotropic model. Central section (80 m from the portals). Contour plots of minimum principal stress magnitude. Contour interval 100 kPa. Lightest color 0-100 kPa. Darkest color 600-700 kPa.

Can. Geotech. J. Downloaded from www.nrcresearchpress.com by UNIVERSITAT POLITECNICA DE CATALUNYA on 04/03/18
For personal use only. This Just-IN manuscript is the accepted manuscript prior to copy editing and page composition. It may differ from the final official version of record.

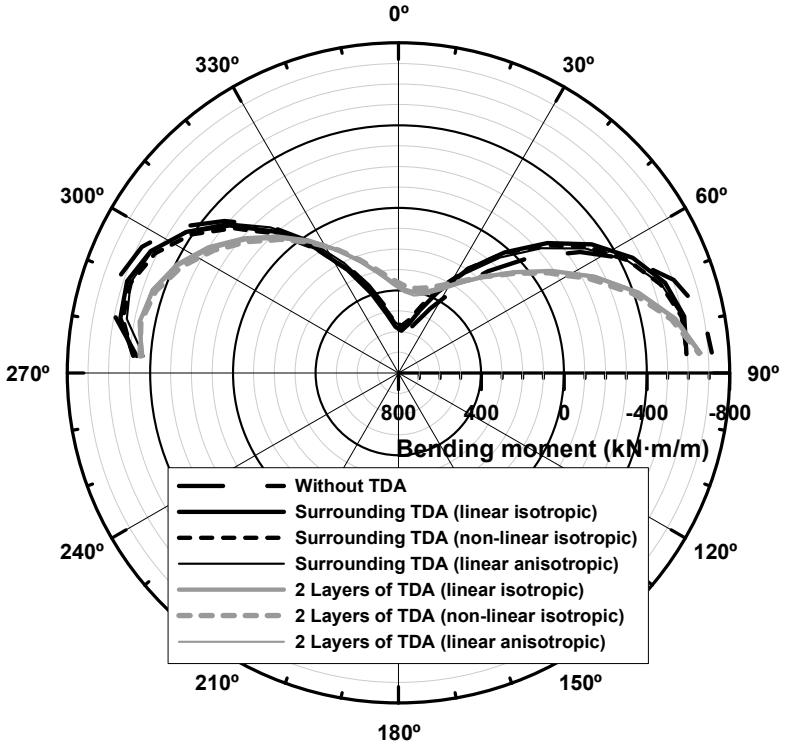

Figure 17 Effect of both different constitutive models and different TDA distributions on computed bending moments.

Can. Geotech. J. Downloaded from www.nrcresearchpress.com by UNIVERSITAT POLITECNICA DE CATALUNYA on 04/03/18
For personal use only. This Just-IN manuscript is the accepted manuscript prior to copy editing and page composition. It may differ from the final official version of record.

Table 1 Gradation of the TDA material

Maximum size (mm)	Percentage Passing (%)
450	100
300	90
200	75
75	50
38	25
4.75	1

Table 2 Readings at earth pressure cells (kPa)

	Section S1	Section S2	Section S3
27/06/2014	46	58	63
26/09/2014	63	112	-
18/10/2014	64	112	-
18/11/2014	67	123	-

Table 3 Final readings at settlement platforms in cm (positive downwards)

	Section S1	**Section S2**	**Section S3**
Plate 1 (below TDA)	33.2	7.2	12.8
Plate 2 (above TDA)	89.5	46	20.5

Table 4 Secant modulus from settlement observations

Material	Section S1	Section S2	Section S3
E_{TDA} (kPa)	517	742	-
E_{fill2} (kPa)	-	-	3,470

Can. Geotech. J. Downloaded from www.nrcresearchpress.com by UNIVERSITAT POLITECNICA DE CATALUNYA on 04/03/18
For personal use only. This Just-IN manuscript is the accepted manuscript prior to copy editing and page composition. It may differ from the final official version of record.

Table 5 Mechanical properties adopted for the non-TDA materials

	γ (kN/m^3)	E (kPa)	ν	φ(º)	c(kPa)
Substrate	26	10^6	0.25	40	800
Fill 1	19	10,000	0.30	35	0
Fill 2	18	3,470[a]	0.30	25	5
Rockfill	22	200,000	0.30	45	200
Concrete	24	$3 \cdot 10^7$	0.20	-	-

Table 6 Mechanical properties adopted for the TDA layer

Model	γ (kN/m^3)	E (kPa)	ν	a*	b	E_{11} (kPa)	E_{33} (kPa)	ν_{12} ($=\nu_{31}$)	ν_{13}
linear isotropic	6.4	630	0.20	-	-	-	-	-	-
non-linear isotropic	6.4		0.20	248	2.65	-	-	-	-
linear anisotropic	6.4	-	-	-	-	946	630	0.11	0.37

In all models the Mohr-Coulomb properties are: φ =23º, c=10 kPa
*Parameters a and b for equation (2)